Available online at www.sciencedirect.com
ScienceDirect
Journal of Solid State Chemistry 180 (2007) 818–823
JOURNAL OF SOLID STATE CHEMISTRY
www.elsevier.com/locate/jssc

Tight binding prediction of the α-Gd_2S_3 magnetic structure

Lindsay E. Roy, Timothy Hughbanks*

Department of Chemistry, Texas A&M University, P.O. Box 30012, College Station, TX 77842-3012, USA

Received 31 August 2006; received in revised form 17 November 2006; accepted 23 November 2006
Available online 12 December 2006

Abstract

Spin-dependent extended Hückel tight binding (EHTB) calculations were carried out for the magnetic solid Gd_2S_3 by considering 20 different variations in the ordering of the $4f^7$ moments. The tight-binding calculations are used to interpolate the band structure of a nonmagnetic congener (Y_2S_3) and the $4f/5d,6s$ exchange interactions are introduced as perturbations via the introduction of spin-dependent H_{dd} and H_{ss} parameters. The calculations predict that Gd_2S_3 adopts an antiferromagnetic ordering of the $4f^7$ moments that is consistent with published neutron diffraction results. Our attempt to account for the calculated energies of the spin patterns using an Ising model was unsuccessful.

Keywords: DFT; Extended Hückel; Broken symmetry approach; Rare-earth magnetism

1. Introduction

The magnetic properties of α-Gd_2S_3 have captured the interest of several research groups [1–4]. This compound has an orthorhombic structure (*Pnma*) wherein two types of cation polyhedra which are linked to form a three-dimensional (3D) structure [2,5,6]. The crystal structure of α-Gd_2S_3 projected onto the *ac* plane is shown in Fig. 1. One cation resides in an eight-coordinate bicapped trigonal prism (BTP) formed by the eight surrounding sulfur atoms (Fig. 2A) and seven sulfur atoms form a distorted monocapped trigonal prism (MTP) around the other cation (Fig. 2B).

There are five structure types for Ln_2S_3 (Ln = lanthanides), two of which are known for Gd_2S_3: α-Gd_2S_3 and γ-Gd_2S_3. The latter has a Th_3P_4-type structure ($I\bar{4}3d$) where 1/9th of the sites of the metal sublattice are vacant [7–9]. Until recently, interest in the magnetic and electrical properties at low temperatures have focused on the γ-type structure. Although γ-Gd_2S_3 exhibits antiferromagnetic ordering with a Néel temperature near 4 K, excess Gd leads to giant magnetoresistance (GMR) or, at higher Gd contents, an antiferromagnet–ferromagnet transition concomitant with a semiconductor–metal transition [10–15].

Researchers have recently reported that α-Gd_2S_3 exhibits an antiferromagnetic transition at $T_N = 10$ K and semiconducting behavior for electronic transport along the *b*-axis [2], though there were previous reports of Curie–Weiss behavior down to 4.2 K with a Weiss constant of −8 K—i.e., no magnetic ordering was reported [5,6,16]. However, heat capacity measurements on a single crystal sample of α-Gd_2S_3 shows a sharp anomaly at $T_N = 9.8$ K, indicative of long-range magnetic ordering [1]. Magnetic susceptibility measurements for the single crystal showed that χ with the applied field parallel to the *b*-axis exhibits a sharp decrease at about 10 K, while the susceptibility with the field perpendicular to the *b*-axis steadily increases with decreasing T [2]. Ebisu et al. interpreted this anisotropic behavior in the T dependence of χ on the basis of a coupled two-leg spin ladder model. To determine the magnetic structure and study the effects of magnetic frustration, neutron diffraction experiments were performed on powder samples of α-$^{160}Gd_2S_3$ [3]. Results show that the magnetic cell is the same as the structural unit cell where the magnetic moments aligned parallel along the *b*-axis [3]. Matsuda et al. proposed the ordering in the *ac* plane by finding the best match between observed magnetic intensities and those calculated for various alternative spin

*Corresponding author. Fax: +1 979 847 8860.
E-mail address: trh@mail.chem.tamu.edu (T. Hughbanks).

0022-4596/$ - see front matter © 2007 Published by Elsevier Inc.
doi:10.1016/j.jssc.2006.11.035

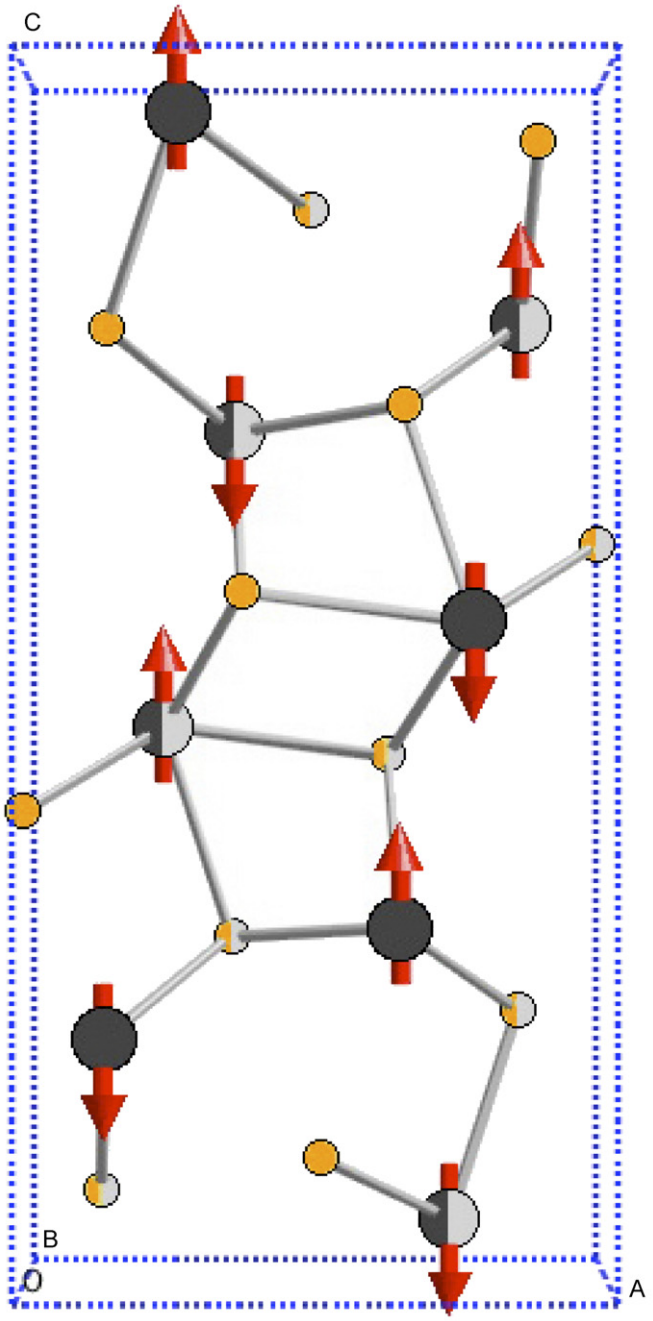

Fig. 1. The crystal structure and proposed magnetic structure of α-Gd_2S_3 projected onto the *ac* plane [3]. Gd atoms are large circles and S atoms are small circles. The solid circles represent the atoms at $y = \frac{1}{4}$ and the two-tone circles represent the atoms at $y = \frac{3}{4}$.

pattern arrangements (Fig. 1) [3]. Independent synchrotron X-ray diffraction studies in zero and non-zero applied fields supports these findings [4].

Electronic band structure calculations for α-Gd_2S_3 have not been reported. In recent years, we have shown that spin density functional theory (SDFT) is useful for studying interatomic exchange coupling in gadolinium-containing molecules and solids [17–21]. Our approach consists of calculating the relative energies of competing "spin patterns" in order to deduce the nature of coupling in

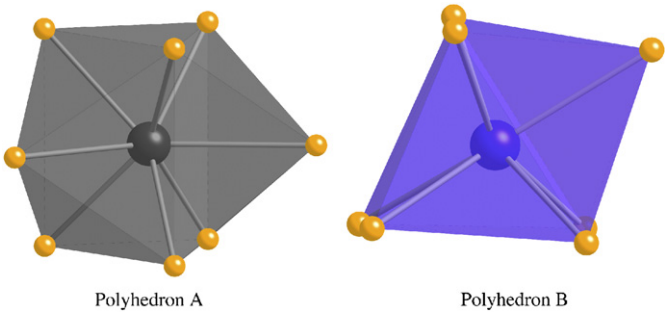

Fig. 2. Coordination polyhedra in α-Gd_2S_3. Left: GdS_8 bicapped trigonal prism. Right: GdS_7 monocapped trigonal prism.

both discrete polynuclear and extended structures. Recently, we have developed a spin-dependent extended-Hückel tight binding (EHTB) method that can be used to predict the magnetic structure of Gd-containing solids where SCF convergence has been difficult to achieve [21]. In the present work, we probe the magnetic structure of α-Gd_2S_3 using our spin-dependent EHTB method.

2. Simulating *d*-electron mediated *f–f* exchange

Lanthanide atoms or ions with $4f^n5d6s^2$ or $4f^n5d$ configurations exhibit substantial intraatomic exchange interactions between 4*f* and valence 5*d* and 6*s* electrons. In the case of the Gd^{2+} ion, for example, the energetic costs of flipping the spin of a 5*d* or 6*s* electron in opposition to the $4f^7$ spins are 1.16 and 0.29 eV, respectively (Fig. 3) [22].

The intraatomic exchange interaction is intrinsically "ferromagnetic", favoring parallel intraatomic alignment of the valence electrons with the 4*f* electrons. The idea of aligning localized moments via delocalized electrons motivated us to investigate the magnetic properties of lanthanide molecules, clusters, and solids where one or more unpaired and/or delocalized cluster electrons are available. We have previously shown that the use of first principles SDFT calculations within the broken symmetry approach is appropriate for the treatment of magnetic coupling that arises from *d*-electron mediated *f–f* exchange on Gd compounds and solids [17–20,23,24]. However, due to computational (convergence) difficulties experienced in the use of SDFT in using our spin pattern approach on *Ln*-containing conductors (i.e., the partially filled band case), we have recently implemented a tight-binding scheme (in the EHTB formalism) to address such problems. In our approach, EHTB parameters are chosen to reproduce first-principles benchmark results to simulate *d*-electron mediated *f–f* exchange in the model $Gd_6CoI_{12}(OPH_3)_6$ [21]. This has allowed us to circumvent convergence difficulties at a low computational cost. In this paper, we demonstrate that this tight-binding model is applicable to insulators as well.

The electronic structure of the nonmagnetic congener, Y_2S_3, was first considered; electronic band calculations for Y_2S_3 were performed at the semi-empirical and first

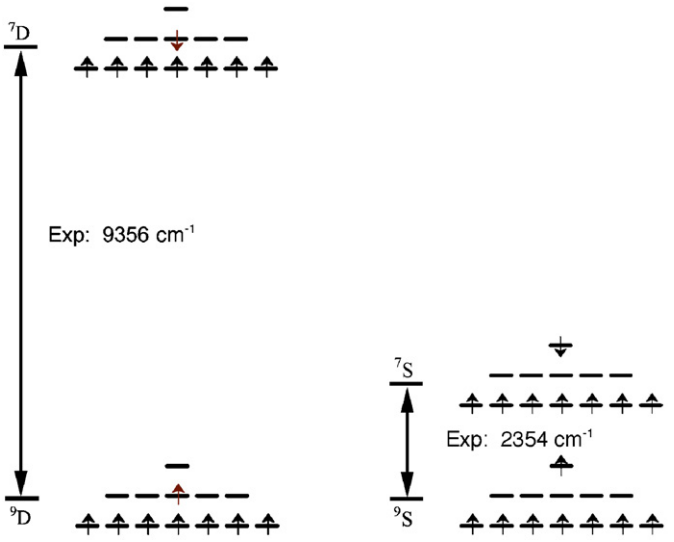

Fig. 3. The *d–f* and *s–f* exchange interactions for the Gd^{2+} ion. The Gd^{2+} ion ground state (^{9}D) and the ^{7}D, ^{9}S, and ^{7}S excited states have predominantly the 4*f*/5*d*/6*s* orbital character illustrated.

principles levels of theory. Despite its semi-empirical nature, the EHTB approach has been successful in providing a semi-quantitative description of the magnetic coupling found in transition metal magnetic molecules and solids [25,26]. In our EHTB calculations, the 4*f* orbitals on a lanthanide atoms are not explicitly included and it is generally understood that they play a minor role in bonding. Nevertheless, an adaptation of the method provides a means for interpreting the magnetic properties of Gd-containing compounds. The basis for our procedure has been published [21], but in outline, it is as follows: We use density functional theory (DFT) band calculations to provide a first-principles description of a nonmagnetic member of this series of compounds (i.e., Y_2S_3). Parameters for EHTB calculations (H_{ii}'s) are adjusted to simulate as closely as possible the DFT band structure for this compound. Exchange effects exerted by the 4*f* moments are included in the EHTB calculations as a spin-dependent perturbation to the Gd atom 5*d*- and 6*s*-orbital energies (H_{dd} and H_{ss}). For a Gd atom with *up-spin* 4*f* electrons, labeled "Gd^+"("Gd^-"), the up-spin (down-spin) 5*d*/6*s* electrons are assigned more (less) negative 5*d*/6*s* orbital energies in the tight-binding approach. Of course, the situation is reversed for a Gd atom with *down-spin* 4*f* electrons: the up-spin (down-spin) 5*d*/6*s* electrons are assigned less (more) negative 5*d*/6*s* orbital energies.

The tight-binding calculations are carried out as follows: (a) for a ferromagnetic spin-pattern (all up-spin Gd centers), two EHTB calculations are performed: one with parameters appropriate for up-spin 5*d*/6*s*-electrons and one for down-spin 5*d*/6*s*-electrons. The Fermi levels for the two calculations are set equal and chosen such that the total number of electrons for the system is appropriate; (b) for an antiferromagnetic 4*f*-spin-pattern where all the Gd atoms are crystallographically equivalent (and the magnetic structure is equivalent to its antistructure), only a single EHTB calculation is required since the up- and down-spin 5*d*/6*s* electron band structure is the same. In this case, of course, the *local* spin 5*d*/6*s* polarizations are *not* the same, but when summed over all atoms, the up- and down-spin 5*d*/6*s* populations are the same; (c) for an antiferromagnetic 4*f*-spin-pattern where all the Gd atoms are not crystallographically equivalent, the up- and down-spin 5*d*/6*s* electron band structure are not the same and two EHTB calculations must be performed and handled as in the ferromagnetic case.

3. Electronic structure of α-Y_2S_3 and magnetic ordering in α-Gd_2S_3

Fig. 4b shows the resulting DOS for electronic structure calculations using the yttrium analog, Y_2S_3, at the semi-empirical and first principles level of theory. The plots of the partial density of states (PDOS) calculated for the Y atom are also presented in Fig. 4. The correspondence between the EHTB and DFT calculations is good; the S *p*-levels and Y *d*-levels have approximately the same bandwidth and the conduction band begins at approximately the same relative energies. Our calculations yield the expected semiconducting behavior, with an energy gap of ~2.4 eV separating the primarily S *p*-levels from the primarily Y *d*-levels. The S *p*-levels have a modest Y-*d* admixture; 12% of the *d*-based orbitals are filled up to the Fermi level for the MTP and BTP yttrium clusters, indicating modest covalence in the Y–S bonding. Although both clusters contain different coordination environments,

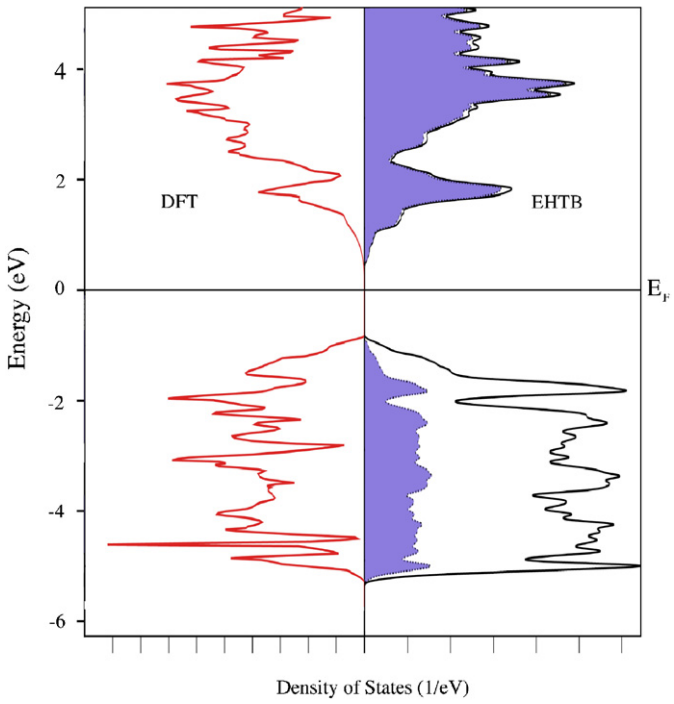

Fig. 4. DOS plot for α-Y_2S_3 for DFT and EHTB calculations. The Y contribution is shaded.

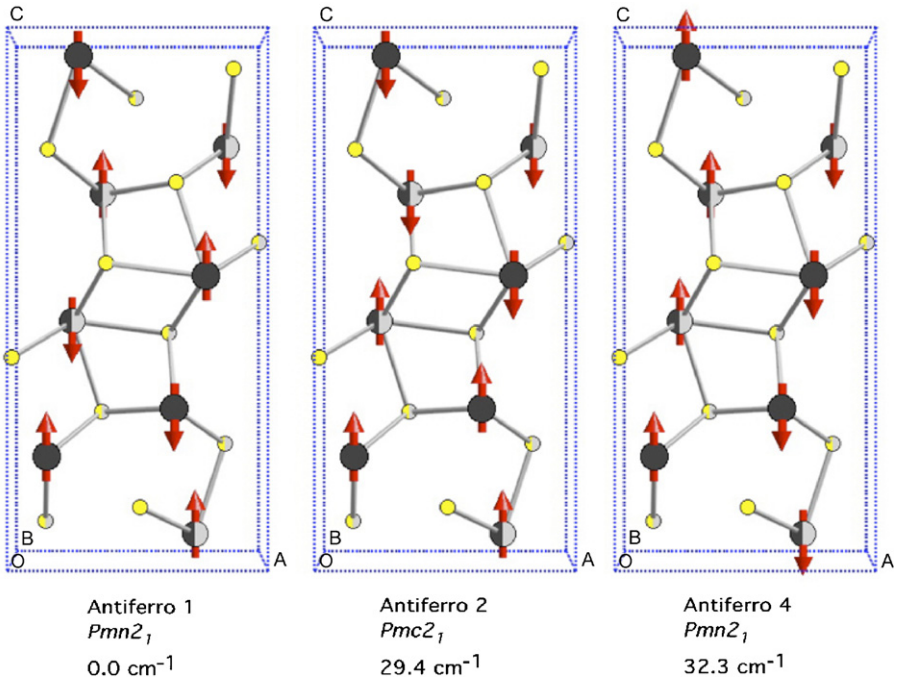

Fig. 5. Three lowest energy spin patterns for "α-Gd_2S_3" [27].

the relative shape of filled levels in the PDOS is (to a first approximation) the same.

To investigate the magnetic ordering in α-Gd_2S_3, we carried out electronic band calculations using the spin-dependent EHTB method for 20 possible spin patterns arrangements: one ferromagnetic and 19 antiferromagnetic [3]. Two calculations were necessary for the ferromagnetic and Antiferro7 spin patterns. Because the neutron diffraction experiments determined that the magnetic cell is the same as the crystallographic cell, we focus our discussion on the possible spin patterns that are non-isomorphic subgroups of the chemical space group *Pnma* [27]. Fig. 5 depicts the three lowest energy spin patterns belonging to subgroups of *Pnma*. The lowest spin pattern is the same as the magnetic structure proposed by Matsuda et al. [3]. The Gd moments adopt antiferromagnetic alignment among atoms within their respective *ac*-planes.

Using fragments based on structures of metal-rich gadolinium compounds, we have previously shown that open-*d*-shell clusters facilitate strong ferromagnetic coupling whereas closed-*d*-shell systems prefer antiferromagnetic coupling [17–20]. The qualitative features can be interpreted using a perturbative molecular orbital (PMO) model that focuses on the influence of the $4f^7$–*d* exchange interaction on the *d*-based molecular orbitals. In view of our foregoing discussion, it is not surprising that α-Gd_2S_3 orders antiferromagnetically given that this solid is an ordinary Gd^{III} compound (a large-gap semiconductor with no *d*-electrons). Our calculations predict semiconducting behavior and calculated gap is nearly equal (~2.2 eV) for antiferro1 and ferromagnetic spin patterns and the spin-polarization of the occupied bands is quite modest, since they have ⩽25% metal character (see Fig. 4). DOS plots (or plots of dispersion curves, for that matter) do not reveal the source of the relative stabilization of the observed antiferromagnetic spin pattern vs. the ferromagnetic spin pattern—we should not expect the small exchange energy preference to show up in a DOS plot that spreads over several electronvolts.

From the computed results for 20 spin patterns, one may compute 19 independent energy differences using the lowest energy spin pattern from EHTB results and each difference may be set equal to an Ising parameter expression. As we concluded in our study of Gd_2Cl_3 and GdB_2C_2, an Ising model is inappropriate for describing the weak exchange. It is nevertheless surprising that a pairwise exchange model fails even for this closed shell compound. This may be a result of the spin frustration in the square and triangular Gd networks formed in the structure.

4. Concluding remarks

Recently, we have found that careful parameterization of EHTB calculations which simulate 5*d*/6*s*–4*f* spin polarization from DFT calculations can correctly predict magnetic structures of Gd-containing metallic systems. The present study reports the extension of our spin-dependent EHTB method to a wide-gap semiconductor. Our calculations have been able to correctly predict the magnetic structure determined from neutron diffraction experiments, and this success illustrates that the *underlying basis* of the RKKY interaction, the intraatomic 5*d*/6*s*–4*f* exchange interaction, can be applied to insulators as well as electronic conductors. The Gd moments adopt antiferromagnetic alignment among nearest neighbor atoms within their respective *ac*-planes. An Ising model does not provide an

Table 1
Extended Hückel exponents (ζ), valence shell ionization potential (H_{ii}'s in eV), and coefficients

Atom	Orbital	H_{ii} (eV)	ζ_1	ζ_2	c_1	c_2
S	3*s*	−20.0	2.1220			
	3*p*	−10.7	1.6370			
Y	5*s*	−7.02	1.74			
	5*p*	−4.40	1.70			
	4*d*	−6.80	1.40	3.60	0.8316	0.3041
"Gd^+"[a]	5*s*	−7.12	1.74			
	5*p*	−4.40	1.70			
	4*d*	−7.03884	1.40	3.60	0.8316	0.3041
"Gd^-"[a]	5*s*	−6.91	1.74			
	5*p*	−4.40	1.70			
	4*d*	−6.56116	1.40	3.60	0.8316	0.3041

[a]Gd^+ and Gd^- are used to model the spin-dependent energies of valence *s* and *d* electrons for Gd centers with spins that are, respectively, aligned parallel and antiparallel with the local spin direction of the 4*f* electrons.

adequate description of the coupling, possibly due to the spin frustration in the square and triangular Gd networks formed in the structure.

Acknowledgments

We thank the Robert A. Welch Foundation for its support through Grant A-1132, the National Science Foundation through Grant DMR-0606629, and the Laboratory for Molecular Simulation at Texas A&M University for computing time and other support.

Appendix A

Electronic structure calculations for Y_2S_3 were performed using DFT with the Becke exchange functional and Lee–Yang–Parr (BLYP) correlation functional [28,29]. All DFT calculations presented here were performed using the DMol^3 program from the Materials Studio® suite of programs. The double numerical basis including *d*-polarization functions, DND, was employed in DMol^3 calculations for all atoms. For yttrium, a small frozen-core (1*s*2*s*2*p*3*s*3*p*3*d*) effective potential was used. All calculations included scalar relativistic effects and open-shell configurations. Structural parameters were taken from the X-ray crystallographic data for α-Gd_2S_3 [2,6]. The criterion for the energy convergence in DFT calculations was set at 10^{-6} a.u. Band calculations were carried out using a mesh of 12 ***k***-points throughout the Brillouin zone to obtain density-of-states (DOS) and band structure plots of high resolution. DOS plots were generated using Cerius2®.

Extended Hückel tight binding (EHTB) calculations were carried out with the program YAeHMOP on α-Y_2S_3 and "α-Gd_2S_3" (simulating (5*d*/6*s*)–*f* spin polarization in α-Gd_2S_3 using a α-Y_2S_3 model). The exponents (ζ's) and valence shell ionization potentials (H_{ii}'s in eV) are listed in Table 1. We used a 1000 ***k***-point mesh in the irreducible wedge of the Brillouin zone. Double-zeta Slater-type orbitals were used to represent Y 4*d* atomic orbitals. The band dispersion and density of states (DOS) diagrams were generated with the viewkel routine.

Appendix B. Supplementary materials

Supplementary data associated with this article can be found in the online version at doi:10.1016/j.jssc.2006.11.035.

References

[1] A. Kikkawa, K. Katsumata, S. Ebisu, S. Nagata, J. Phys. Soc. Jpn. 73 (2004) 2955.
[2] S. Ebisu, Y. Iijima, T. Iwasa, S. Nagata, J. Phys. Chem. Solids 65 (2004) 1113.
[3] M. Matsuda, A. Kikkawa, K. Katsumata, S. Ebisu, S. Nagata, J. Phys. Soc. Jpn. 74 (2005) 1412.
[4] K. Katsumata, A. Kikkawa, Y. Tanaka, S. Shimomura, S. Ebisu, S. Nagata, J. Phys. Soc. Jpn. 74 (2005) 1598.
[5] A.W. Sleight, C.T. Prewitt, Inorg. Chem. 7 (1968) 2282.
[6] C.T. Prewitt, A.W. Sleight, Inorg. Chem. 7 (1968) 1090.
[7] J. Flahaut, M.M. Guittard, M. Patrie, Bull. Soc. Chim. Fr. (1959)1917.
[8] M. Picon, L. Domange, J. Flahaut, M. Guittard, M. Patrie, Bull. Soc. Chim. Fr. 2 (1960) 221.
[9] W.H. Zachariasen, Acta Crystallogr. 2 (1949) 57.
[10] D.G. Andrianov, S.A. Drozdov, G.V. Lazareva, N.M. Ponomarev, V.I. Fistul, Fiz. Nizk. Temp. 3 (1977) 497.
[11] D.G. Drozdov, S.A. Lazareva, G.V. Ponomarev, N.M. Zh, Eksp. Teor. Fiz. 75 (1978) 2228.
[12] D.G. Andrianov, S.A. Drozdov, G.V. Lazareva, Fiz. Tverd. Tela 21 (1979) 2179.
[13] G. Becker, J. Feldhaus, K. Westerholt, S. Methfessel, J. Magn. Magn. Mater. 6 (1977) 14.
[14] S. Washburn, R.A. Webb, S. Von Molnar, F. Holtzberg, J. Flouquet, G. Remenyi, Phys. Rev. B: Condens. Matter 30 (1984) 6224.
[15] S. Von Molnar, J. Flouquet, F. Holtzberg, G. Remenyi, Solid-State Electron. 28 (1985) 127.

[16] D.G. Andrianov, G.P. Borodulenko, A.A. Grizik, S.A. Drozdov, V.I. Fistul, Fiz. Tverd. Tela 17 (1975) 1831.
[17] L.E. Roy, T. Hughbanks, Mater. Res. Soc. Symp. Proc. 755 (2002) 25.
[18] L. Roy, T. Hughbanks, J. Solid State Chem. 176 (2003) 294.
[19] L.E. Roy, T. Hughbanks, J. Am. Chem. Soc. 128 (2006) 568.
[20] L.E. Sweet, L.E. Roy, F. Meng, T. Hughbanks, J. Am. Chem. Soc. 128 (2006) 10193.
[21] L.E. Roy, T. Hughbanks, J. Phys. Chem. B 110 (2006) 20290.
[22] NIST Exchange Splitting Energies for Gd. 〈http://physics.nist.gov/cgi-bin/AtData/main-asd〉
[23] L. Noodleman, J. Chem. Phys. 74 (1981) 5737.
[24] L. Noodleman, D.A. Case, Adv. Inorg. Chem. 38 (1992) 423.
[25] M.-H. Whangbo, H.-J. Koo, D. Dai, J. Solid State Chem. 176 (2003) 417.
[26] E.M. Tejada-Rosales, J. Rodriguez-Carvajal, N. Casan-Pastor, P. Alemany, E. Ruiz, M.S. El-Fallah, S. Alvarez, P. Gomez-Romero, Inorg. Chem. 41 (2002) 6604.
[27] All 20 computed spin patterns and their respective energies can be found in supplementary material.
[28] A.D. Becke, Phys. Rev. A: At. Mol. Opt. Phys. 38 (1988) 3098.
[29] C. Lee, W. Yang, R.G. Parr, Phys. Rev. B: Condens. Matter 37 (1988) 785.